




# Bacterial cellulose-based scaffold with in-situ cationic micelle modification for urethral stricture disease: Sustained drug components release, cytokines recruitment, and bacterial microenvironment regulation

Zhenpeng Zhu<sup>a,b,c,d,1</sup> , Jianming Zhao<sup>e,1</sup>, Xing Ji<sup>a,b,c,d,1</sup>,  
Weimin Hu<sup>a,b,c,d</sup>, Wenyan Leng<sup>a,b,c,d</sup>, Chunru Xu<sup>a,b,c,d</sup>,  
Xiaoyu Li<sup>a,b,c,d</sup>, Kunlin Yang<sup>a,b,c,d</sup>, Xuesong Li<sup>a,b,c,d,\*</sup>,  
Yudong Zheng<sup>e,\*\*</sup>, Jian Lin<sup>a,b,c,d,\*\*\*</sup>

<sup>a</sup> Department of Urology, Peking University First Hospital, Beijing, 100034, China

<sup>b</sup> Institute of Urology, Peking University, Beijing, 100034, China

<sup>c</sup> National Urological Cancer Center, Beijing, 100034, China

<sup>d</sup> Beijing Key Laboratory of Urogenital Diseases (Male) Molecular Diagnosis and Treatment Center, Beijing, 100034, China

<sup>e</sup> School of Materials Science and Engineering, University of Science and Technology Beijing, Beijing, 100083, China

## ARTICLE INFO

### Keywords:

Urethral stricture disease  
Bacterial cellulose  
Urethral reconstruction  
Polyurethane  
Antibacterial

## ABSTRACT

The treatment of urethral stricture disease and the prevention of restenosis present considerable challenges in the field of urology. Tissue-engineered materials, particularly bacterial cellulose scaffolds, have emerged as promising solutions due to their abundant sources, excellent mechanical properties, and biocompatibility. However, for attaining superior treatment for patients with USD, further modification of bacterial cellulose is necessary. We have fabricated a dual-network scaffold with enhanced antibacterial properties and cytokines absorption ability through in-situ polymerization of cationic polyurethane micelles and cyclodextrin on oxidized bacterial cellulose. This scaffold also enables long-term sustained release of loaded drug components. Animal model studies have confirmed that this scaffold can achieve urethral repair outcomes comparable to those of normal urethral tissue. This innovative material provides a robust foundation for advancing new concepts and methodologies in the treatment of urethral stricture disease, potentially transforming clinical approaches to this challenging condition.

## 1. Introduction

Urethral stricture disease (USD) represents a significant challenge to the field of urology, with a high prevalence observed in elderly male patients [1,2]. The primary characteristic of USD is extensive fibrosis of the tissue surrounding the urethra consequent to injury or infection [3,4]. In the event of damage to the urethra, the inadequate repair capacity of the epithelial cells can result in the infiltration of inflammatory cells and fibroblasts into the damaged area [5,6], ultimately resulting in the formation of scar and the development of USD. Bacterial urethritis,

which is characterized by a microenvironment teeming with bacteria, is also a contributing factor to the failure of urethral injury repair [7]. Consequently, it is imperative to facilitate early repair of the affected areas, suppress bacterial presence in the microenvironment, and modulate the scar contraction process induced by inflammatory cells and fibroblasts [8,9]. These measures are crucial for the effective treatment of USD [10].

Current clinical treatments for patients with USD typically employ a range of therapeutic modalities, such as drug injections, endoscopic procedures and surgical interventions, with the aim of alleviating

Peer review under the responsibility of editorial board of Bioactive Materials.

\* Corresponding author.

\*\* Corresponding author.

\*\*\* Corresponding author.

E-mail addresses: [pineneedle@sina.com](mailto:pineneedle@sina.com) (X. Li), [zhengyudong@mater.ustb.edu.cn](mailto:zhengyudong@mater.ustb.edu.cn) (Y. Zheng), [linjianbj@163.com](mailto:linjianbj@163.com) (J. Lin).

<sup>1</sup> Dr. Zhu, Dr. Zhao, and Dr. Ji. Are co-first authors.

<https://doi.org/10.1016/j.bioactmat.2025.04.031>

Received 10 February 2025; Received in revised form 10 April 2025; Accepted 25 April 2025

2452-199X/© 2025 The Authors. Publishing services by Elsevier B.V. on behalf of KeAi Communications Co. Ltd. This is an open access article under the CC BY-NC-ND license (<http://creativecommons.org/licenses/by-nc-nd/4.0/>).



disease progression [1,11]. For patients presenting with lengthy and complex urethral strictures, tongue mucosa or buccal mucosa is frequently employed for repair in clinical practice. However, the therapeutic outcome is not satisfactory and is influenced by the quantity of the obtained material and complications at the collection site [12]. Currently, the small intestinal submucosa (SIS) materials utilized clinically exhibit suboptimal therapeutic outcomes for long and complex urethral strictures, and appropriate urethral stent materials remain to be explored [13]. Tissue-engineered materials possess a wide array of sources and can be fully designed and modified, demonstrating broad prospects in the treatment of USD [14,15]. Bacterial cellulose (BC) has become a widely used component in tissue engineering in recent years, due to its characteristics [16,17]. Our previous research confirmed the remedial effects of BC on urethral reconstruction [18]. However, further modification of BC is necessary to fulfill the demands of therapy [19,20]. It has been demonstrated in previous studies that mitomycin C (MMC) has significant potential as an anti-scarring agent in both animal and clinical studies [21,22]. Moreover clinical practices indicate that MMC can provide long-term benefit to patients with USD [23,24]. Controlling the long-term sustained release of MMC can enhance repair outcomes, necessitating further optimization to effectively load MMC onto scaffold [25,26]. Cyclodextrin (CD), a compound with a unique cavity structure, can form inclusion complexes with drug molecules via hydrophobic interactions [27,28]. This encapsulation significantly improves the physicochemical properties of drugs, such as solubility and stability, offering an effective strategy for sustained drug release [29,30]. Utilizing the drug-loading capacity of CD combined with BC, the sustained-release properties of MMC scaffolds can be effectively

achieved.

In our study, we synthesized an oxidized cellulose polyurethane (OBCPU) dual-network scaffold for complex microenvironment regulation of urinary tract stenosis by in-situ polymerization of cationic polyurethane micelles (PU) and vinyl cyclodextrin on the surface of oxidized bacterial cellulose (OBC). PU effectively enhances the surface properties of cellulose and can efficiently adsorb cytokines from the surrounding environment. Additionally, the cationic nature of PU endows OBCPU with significant antibacterial properties. Moreover, leveraging the unique drug-loading capacity of cyclodextrin, we incorporated MMC into OBCPU to achieve sustained release. Using a New Zealand rabbit urethral defect model, we evaluated the therapeutic efficacy of OBCPU, which showed promising results in regulating the bacterial microenvironment and tissue repair. The application of this novel scaffold offers novel insights and methodologies for the treatment of USD (Fig. 1).

## 2. Result

### 2.1. Synthesis and characterization of OBCPU

OBCPU primarily achieved cross-linking through the Schiff base reaction between the amino groups capped with PU and the carbonyl groups of OBC. Simultaneously, the amino group also reacted with the vinyl group on the modified CD to form C-N bonds, thereby creating a dual-network structure (Fig. 2A). The gross images of BC, OBC and OBCPU have been exhibited in Fig. S1. FT-IR revealed a decrease in -OH content within the material and a weakening of the peak at  $3325\text{ cm}^{-1}$ ,

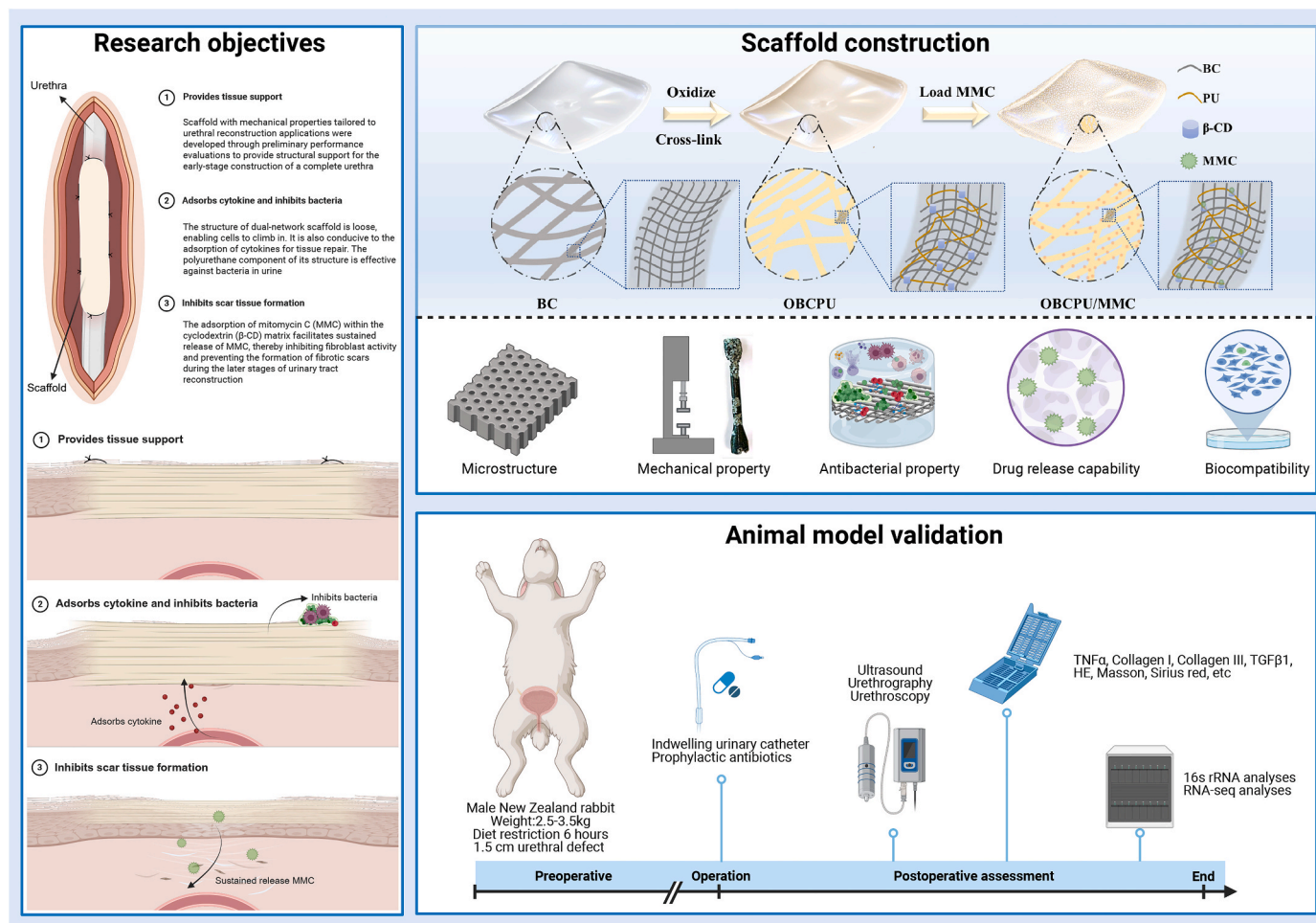
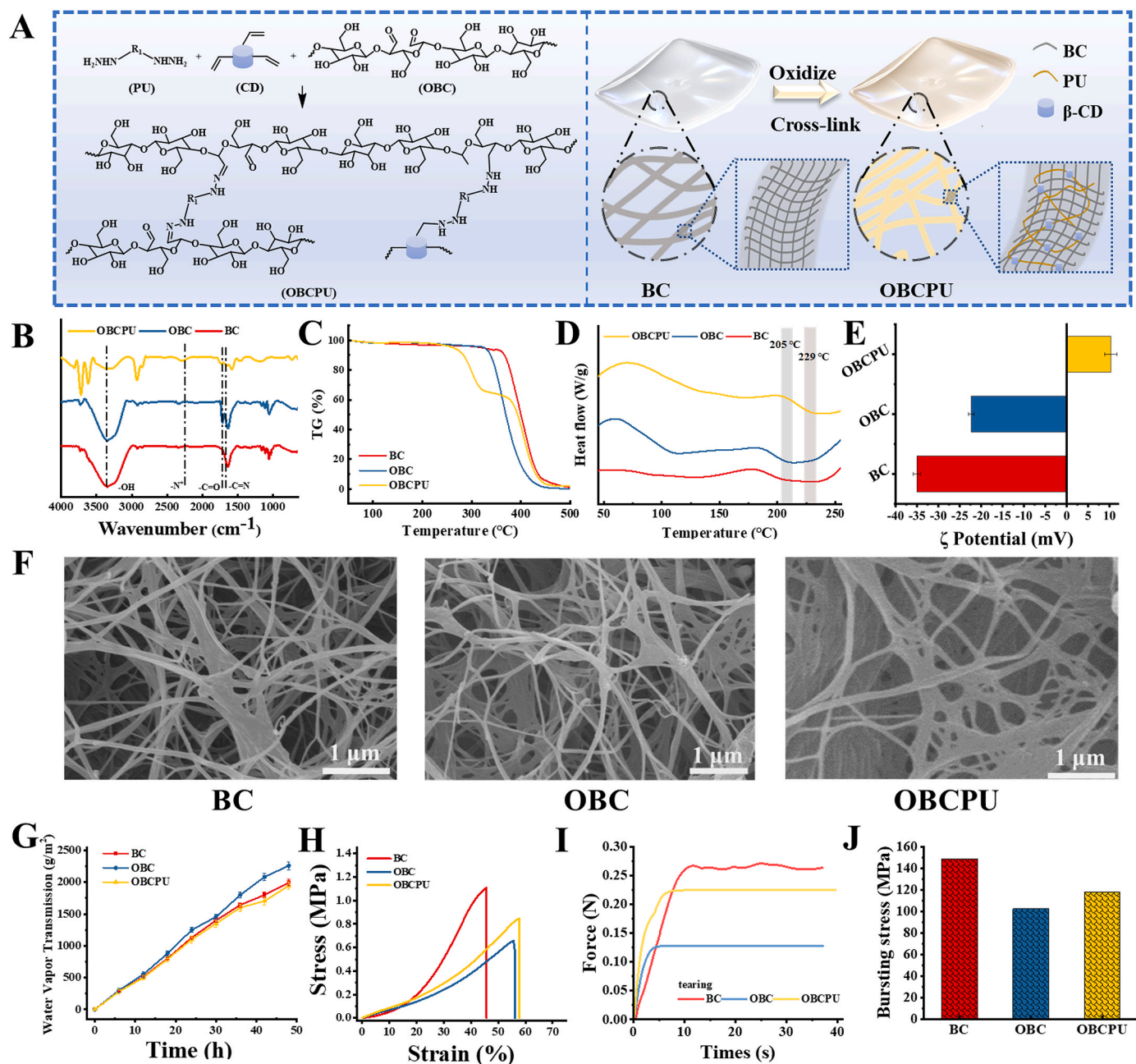


Fig. 1. The flowchart of the whole experiment process.





**Fig. 2.** (A) Synthesis of OBCPU; (B) FT-IR, (C) TG, (D) DSC and (E)  $\zeta$ -potential of BC, OBC and OBCPU; (F) SEM of BC, OBC and OBCPU (scale bar: 1  $\mu$ m); (G) Water vapor transmission, (H) Tensile stress-strain curve, (I) Tear curve and (J) Bursting stress of BC, OBC and OBCPU.

indicating the binding of PU to BC molecules. Moreover, the presence of an  $-N^+$  peak at  $2260\text{ cm}^{-1}$  confirmed the successful modification of PU with a quaternary ammonium salt structure, which underpins the material's antibacterial properties. In the infrared spectrum of OBC, only the  $C=O$  peak at  $1730\text{ cm}^{-1}$  was observed, confirming the successful introduction of carbonyl groups through the oxidation of bacterial cellulose. Meanwhile, the appearance of a  $C=N$  peak at  $1666\text{ cm}^{-1}$  in OBCPU directly indicates the occurrence of the Schiff base reaction. However, these groups were subsequently consumed during PU modification (Fig. 2B). The lack of sharp peaks in XRD suggests that no significant crystallization has taken place. Nonetheless, the peaks from BC at  $19.5^\circ$  and  $29.0^\circ$  were still discernible post-oxidation, suggesting a minimal degree of material oxidation. The peak at  $43.5^\circ$  confirmed the presence of the PU structure following material modification (Fig. S2). TG showed that the material exhibits good thermal stability and will not

decompose even at  $250^\circ\text{C}$ . At the same time, OBCPU showed two decomposition intervals, with the modification of polyurethane structure at  $254^\circ\text{C}$ , which also verified the synthesis of the material (Fig. 2C). DSC showed that the  $T_g$  of the sample increases with the modification of PU on BC, which is due to the interpenetration of the PU network in BC segments. The mobility of molecular chains decreases, which means that a higher temperature is needed for movement. As a result, the glass transition temperature increases from  $205^\circ\text{C}$  to  $229^\circ\text{C}$  (Fig. 2D).  $\zeta$ -potential indicated that a significant presence of oxygen elements on the surface of BC resulted in negative charge characteristics, which persisted even after the oxidation to OBC. Following the modification with positively charged PU, the surface charge of the OBCPU scaffold shifted to positive (Fig. 2E). Due to the modification of PU, the contact angle of OBCPU has been improved compared to BC and OBC (Fig. S3).

SEM observations revealed that slight oxidation did not damage the



three-dimensional network structure of BC, which also endowed the material with good permeability. The permeability of the material, attributed to its porous structure, could be assessed by evaluating the water vapor transmission rate over 48 h. The oxidation of BC resulted in a looser molecular structure. However, due to the modification with PU, the material permeability of OBCPU was lower than that of OBC (Fig. 2F and G).

The unmodified BC exhibits excellent mechanical properties, with a tensile strength of approximately 1.2 MPa. Although the mechanical properties of OBC remain largely unchanged, its toughness decreases from 0.169 MJ/m<sup>3</sup> to 0.144 MJ/m<sup>3</sup>, primarily due to molecular ring fracture and increased brittleness. The crosslinking between PU and OBC enhances the mechanical strength of the material, with OBCPU achieving a tensile strength of 0.84 MPa and an elongation at break of

58.74 %. This indicates that the mechanical strength of the material has been restored (Fig. 2H and S4). For 3 mm thick cellulose, BC could withstand a force of about 0.262 N before tearing. In contrast, OBC, due to structural damage, was more prone to tearing, with only 0.124 N required to rupture the material. However, after PU modification, the OBCPU scaffold gained the ability to resist shear forces, needing 0.228 N to tear, which is sufficient for stable material fixation during tissue repair (Fig. 2I). Furthermore, the bursting strength of OBCPU was tested and found to be 117.54 MPa, ensuring that the material can withstand pressure without damage during the early stages of treatment (Fig. 2J).

The dual network structure of OBCPU can be verified through a simple doping comparison between the molecules used to modify OBC and OBC itself. It can be clearly observed that the C=N structure is present in OBC/PU due to the absence of the Schiff base reaction.

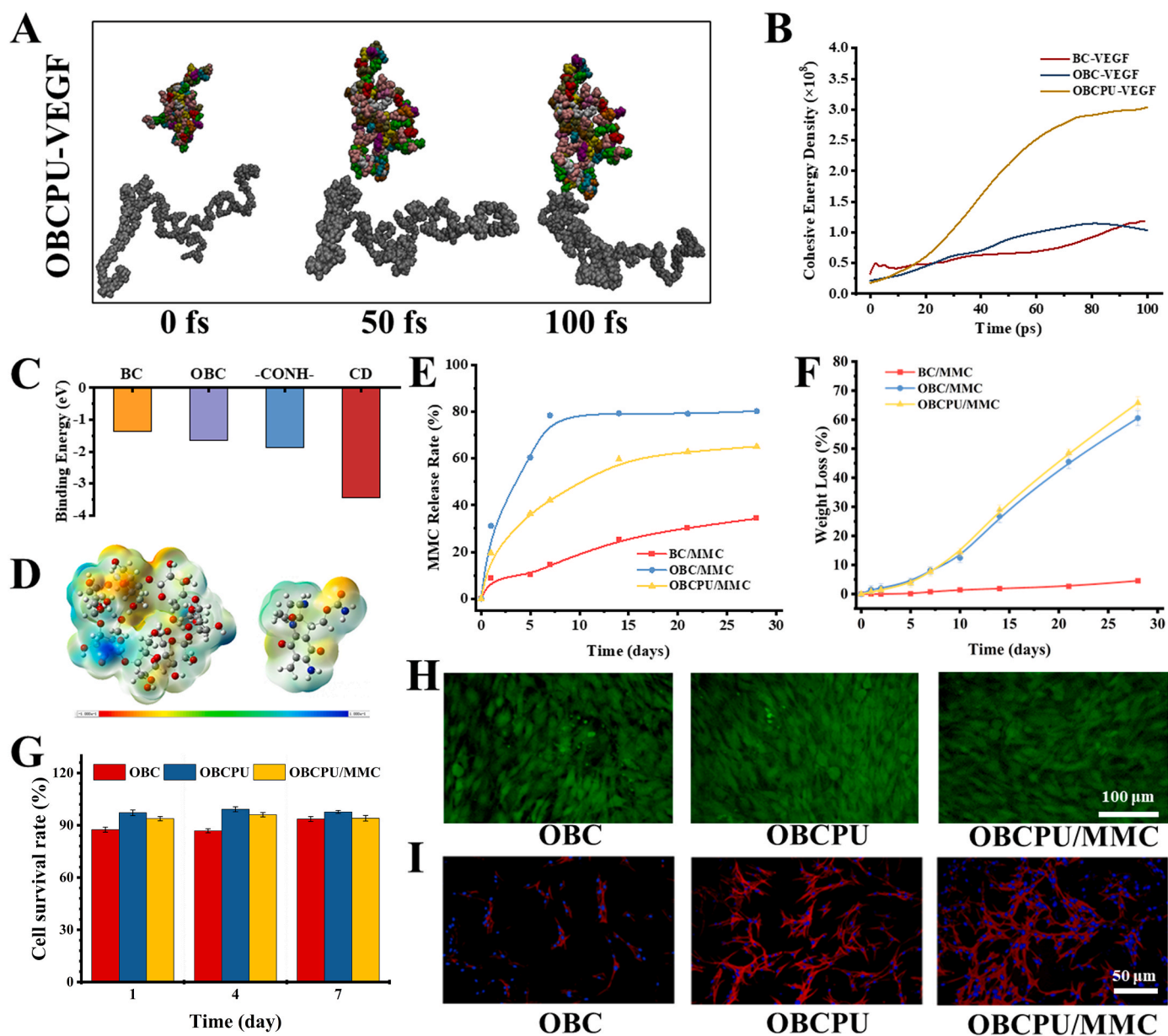


**Fig. 3.** (A) OBCPU captures VEGF within 100fs; (B) Cohesive Energy Density of BC-VEGF, OBC-VEGF and OBCPU-VEGF; (C) Binding Energy of MMC to BC, OBC, -CONH- and CD; (D) Electrostatic Potential Surfaces of  $\beta$ -CD and MMC; (E) MMC release rate of BC/MMC, OBC/MMC and OBCPU/MMC; (F) Weight loss rate of BC/MMC, OBC/MMC and OBCPU/MMC; (G) CCK-8 assay of cell viability; (H) Live and dead staining (scale bar: 100  $\mu$ m); (I) Phalloidin-Rhodamine/DAPI staining of cells on the surface of OBC, OBCPU and OBCPU/MMC (scale bar: 50  $\mu$ m).



Meanwhile, through simple doping, it was evident that the C=O groups were not consumed, and the positive charge density of OBC/PU was relatively low. This type of OBC/PU, which did not form a dual network, exhibited a lower tensile modulus and is more prone to tearing (Fig. S5A–D).

## 2.2. OBCPU's recruitment of small molecules

After being modified by PU, changes were observed in the surface charge and chemical groups of OBCPU. The material effectively captured molecules in the surrounding environment, which facilitated tissue repair by interacting with various tissue factors. To demonstrate this, we used vascular endothelial growth factor (VEGF), a molecule that promotes vascularization and wound healing, to test OBCPU's binding capacity through molecular dynamics simulations.

BC and OBC showed minimal binding to VEGF, with no interaction observed even after movement (Fig. S6). In contrast, OBCPU, featuring a distinct punctual region, gradually bound to VEGF, with mutual attraction noted at 50 fs and molecule contact at 100 fs, resulting in VEGF capture by OBCPU (Fig. 3A). Non-bond interaction analysis revealed significant changes in OBCPU-VEGF non-bond energy, suggesting tighter binding as energy rose during interaction (Fig. S7).

The enhanced adsorption capacity is attributed to the modification of the material by PU. This modification introduces polar groups, such as amino acid esters, into the OBC structure. These polar groups provide additional adsorption sites through electrostatic interactions and hydrogen bonding, improving the material's ability to adsorb other cytokines. The cohesive energy density validated the system's stability and binding capacity, with a notable increase in system cohesive energy due to OBCPU-VEGF interaction. The binding force of OBCPU with VEGF exceeded that of BC and OBC (Fig. 3B), indicating the potential of OBCPU to boost tissue repair by attracting recovery factors, an effect largely due to influence of PU on the material.

## 2.3. Sustained release of MMC

The three-dimensional pores in the cellulose structure allowed for the loading of small molecules, but this physical adsorption lacked stable slow-release properties. Cyclodextrin's macrocyclic structure, however, enabled sustained release through host-guest interactions. The surface electrostatic potential analysis revealed that the positive region of MMC was concentrated in the five-membered ring, which favored its entry into the cyclodextrin cavity and stable loading with the negatively charged region. Binding energy results indicated that the affinity between MMC and CD was significantly higher than that between MMC and BC. The presence of the amino ester structure in OBC or PU suggests that MMC was more effective in loading CD for sustained release, rather than being adsorbed by the fibers (Fig. 3C and D).

The low drug release rate within four weeks was due to BC's resistance to degradation, leading to substantial MMC adsorption. The drug release of OBC/MMC was linked to degradation of OBC, ceasing around the seventh day, indicating no further drug release. Although the weight loss was merely 10 %, the attached MMC was essentially released completely as a result of the extensive disintegration of the OBC/MMC that initiated to occur. In contrast, OBCPU/MMC showed a gradual drug release over time, attributed to drug loading in the cyclodextrin unit, the absence of complete material degradation during the release process, and no drug adsorption by fibers preventing environmental release (Fig. 3E and F). Compared with OBCPU without CD, the MMC release of OBCPU without CD lost its sustained release effect, and the drug loading rate is significantly lower (Fig. S8).

## 2.4. Biocompatibility and cell adhesion efficiency

The cell survival rates for OBC, OBCPU, and OBCPU/MMC exceeded 90 %, confirming the long-term biocompatibility of these materials.

Live/dead staining verified that the materials and MMC had minimal effects on cell viability, despite the observed robust cell growth and high cell counts (Fig. 3G and H). Only a small degree of cell adhesion was observed after 24 h of cell culture on thin film materials. However, OBCPU, modified with PU, showed significantly better cell adhesion, which promoted cell growth. By day 7, the cell count on OBCPU surfaces had doubled compared to OBC surfaces (Fig. 3I and S9). The glucose consumption measurements revealed that OBCPU had a significantly higher consumption rate than OBC. This high glucose intake and metabolic activity may be due to the compatibility of the fiber and porous structures with the cell growth environment, enhancing cell adhesion, diffusion, and proliferation. The PU modification improved cell adhesion, further facilitating cell growth in response to the environment (Fig. S10).

## 2.5. In vitro antibacterial activity

The quaternary ammonium salt structure within PU contributes to its ability to significantly inhibit the growth of *E. coli* in the urinary tract environment, whereas OBC alone does not exhibit notable antibacterial properties. In contrast, the loading of MMC has minimal impact on the antibacterial performance of OBCPU. Both OBCPU and OBCPU/MMC demonstrate significant antibacterial rings. However, the inhibitory effect of OBCPU on *E. coli* is only slightly higher than that of OBCPU/MMC, indicating that both materials possess considerable antibacterial efficacy against this pathogen (Fig. 4A). Observations revealed substantial *E. coli* growth on OBC, whereas minimal adhesion was noted on OBCPU and OBCPU/MMC surfaces. OBCPU also demonstrated effective *E. coli* elimination capabilities (Fig. 4B). Colony counting confirmed that OBCPU and OBCPU/MMC treatments nearly eradicated the bacteria. Although MMC slightly reduced the antibacterial efficacy, OBCPU/MMC still maintained a high antibacterial rate, slightly lower than OBCPU, effectively killing the bacteria (Fig. 4C and D). OBC allowed clear *E. coli* biofilm formation, which was significantly disrupted by OBCPU and OBCPU/MMC into smaller fragments or even disappeared. The antibiofilm efficiency of OBCPU and OBCPU/MMC reached 78.2 % and 81.1 %, respectively, within 24 h, as detected by biofilm activity assays (Fig. 4E and F). Meanwhile, similar antibacterial effects can also be observed on *S. aureus* (Fig. S11).

## 2.6. In vivo therapeutic effects analyzed through imaging and histology

Before conducting the in vivo experiments, we sacrificed healthy New Zealand rabbits and obtained urethral tissues for comparison of mechanical properties with the OBCPU materials. OBCPU exhibits the closest toughness to the urethra, which is beneficial for the material to provide long-term mechanical support during the treatment process (Fig. S12).

At the end point, the corresponding imaging examination was conducted. Firstly, the ultrasound of the urinary tract was performed on the model animals. The ultrasonic results indicated that the injury site in the control group presented bright spots similar to fibrous scars and a relatively narrow diameter, whereas the OBC group had a slightly wider diameter, and the fibrous scars were almost imperceptible. Simultaneously, the lumen of the OBCPU or OBCPU/MMC group was not distinguishable from that of the normal urethra, and the diameter was close to that of the normal urethra (Fig. 5A). Subsequently, the urethroscopy results displayed the results more clearly. In the control group, urethral stenotic tissue was observable, while in the OBC group, there was a small amount of urethral exudate and unevenness. In the OBCPU and OBCPU/MMC groups, the morphology of the urethra was similar to that of a normal urethra, and no obvious abnormalities were detected. The OBCPU/MMC group appeared to be superior to the OBCPU group (Fig. 5B). Finally, an urethrography was carried out, which demonstrated that the OBCPU and OBCPU groups had excellent urethral integrity and continuity, while the OBC group had poor imaging



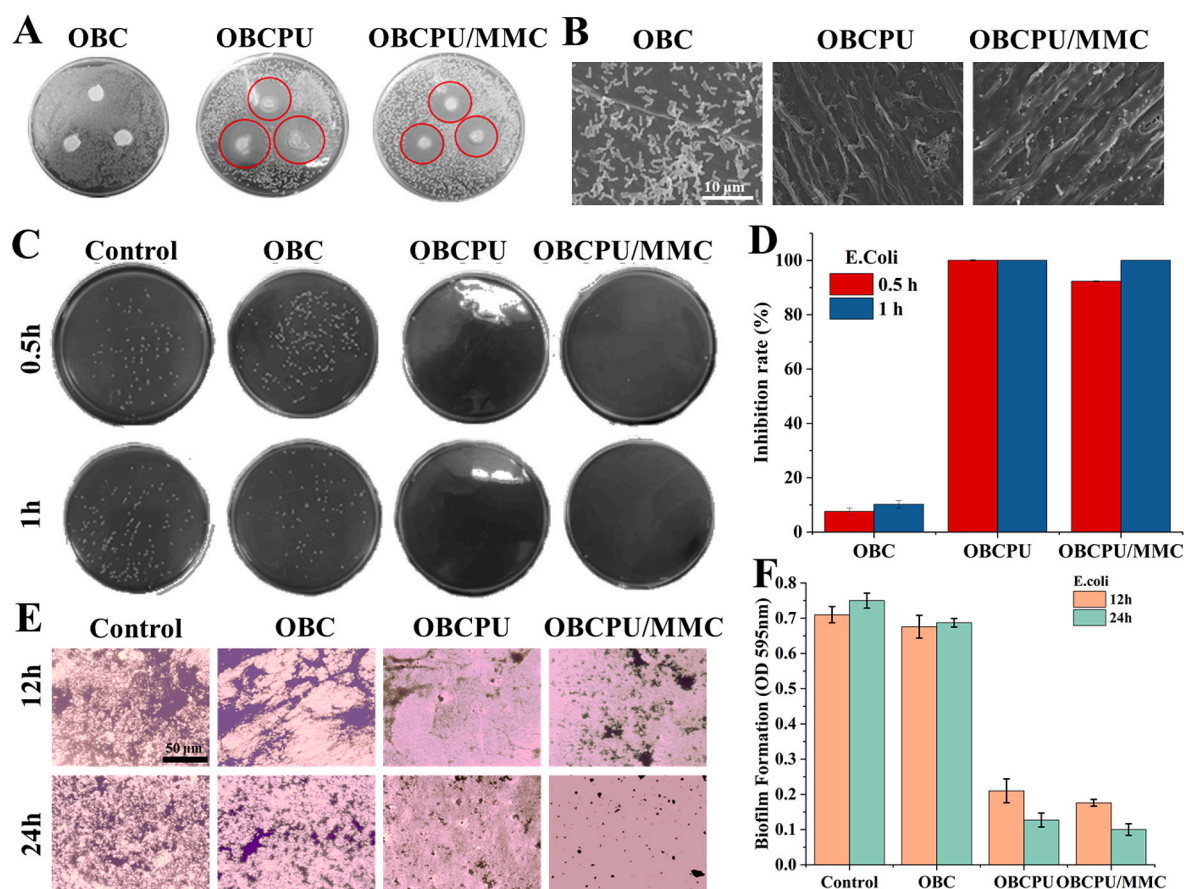


**Fig. 4.** The inhibitory effect of materials on *E. coli*: (A) Antibacterial ring; (B) SEM of bacterial morphology (scale bar: 10  $\mu\text{m}$ ); (C) Antibacterial bacterial morphology; (D) Inhibition rate; (E) Crystal violet (scale bar: 50  $\mu\text{m}$ ); (F) Biofilm absorbance.

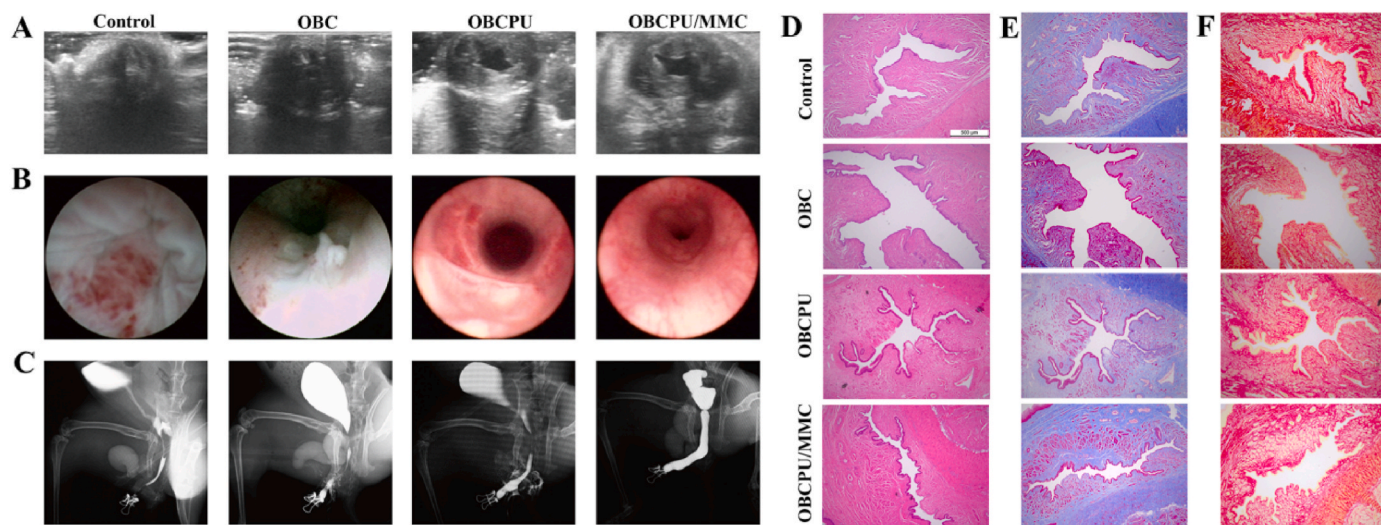


**Fig. 5.** Radiological and histological results of animal models: (A) Ultrasound; (B) Urethroscopy; (C) Urethrography; (D) HE staining (scale bar: 500  $\mu\text{m}$ ); (E) Masson staining (scale bar: 500  $\mu\text{m}$ ); (F) Sirius Red staining (scale bar: 500  $\mu\text{m}$ ).

continuity at the repair site, and the control group exhibited more severe stenosis (Fig. 5C).

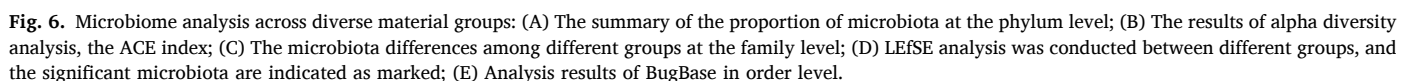
To further assess the repair effect of the scaffold, postoperative histological verification was conducted at the end point. No infections were identified in any of the rabbits in the material group prior to the conclusion of the experiment, suggesting the excellent biocompatibility

of the material. HE staining revealed that, in contrast to the control group, the epithelial coverage in the OBC group was thicker and more complete, while the epithelial coverage in the OBCPU and OBCPU/MMC groups was closer to normal urethral tissue than that in the OBC group, and more vascular tissue could be observable (Fig. 5D). Subsequently, Masson and Sirius red staining were performed to determine the



expression level of TGF $\beta$ 1 in the OBCPU/MMC group was lower, and  $\alpha$ SMA indicated that the smooth muscle was more regular, approximating the normal urethral level (Fig. S13).

Subsequently, 16s rRNA sequencing was conducted to analyze the alterations in flora disparities among urethral tissues repaired with diverse materials and the potential molecular biological mechanisms. Firstly, the number of features in different groups of samples was





counted, and the proportion of distinct flora in the samples at the family level was analyzed (Fig. 6A and Fig. S14A). Subsequently, the  $\alpha$ -diversity of the flora showed that more microbial abundance was visible in the urethral tissue of the OBC group compared to the OBCPU or OBCPU/MMC group, while there was little difference between the OBCPU and OBCPU/MMC groups (Fig. 6B). There are more characteristic numbers in Group 1 (Fig. S14B). The relevant results are similar to those of the in vitro experiments, and MMC does not affect the antibacterial effect. Finally, we performed a differential flora analysis, and we found that the number of pathogenic flora in the OBC group increased significantly, while the OBCPU or OBCPU/MMC group had more regular flora (Fig. 6C). Subsequently, we carried out  $\beta$ -adversity analysis. It can be observed from the NMDS analysis and Binary Jaccard correction analysis that there are significant disparities among the three groups of data, with a correlation of 0.24 (Fig. S14C). We compared the microbiota conditions between different groups at the family level. Enterobacteriaceae exhibited significant differences between the OBCPU and OBC groups. Nevertheless, due to the inadequate sample size, although there were differences in the average values between the OBCPU/MMC group and the OBC group, they were not statistically significant. The relevant results were in accordance with the in vitro experiments. At the Phylum level, a Ternary analysis was conducted, and it was found that Group 2 might have a greater abundance of Firmicutes bacteria, while Group 1 had more Bacteroidota microbiota (Fig. S14D). Simultaneously, LEfSE analysis indicated that the characteristic Enterobacteriaceae bacteria were significant in Group 1, while the Firmicutes microbiota was characteristic in Group (Fig. 6D). Finally, through BugBase analysis, Group 1 was more enriched in Forms\_Biofilms, Potentially\_Pathogenic, Contains\_Mobile\_Elements and Facultatively\_Anaerobic (Fig. 6E).

## 2.8. Potential biological pathway enrichments

Firstly, we acquired RNA-seq data for differential expression analysis, constructed volcano plots and labeled the five genes with the most significant p-values. We discovered that in contrast to the OBC group,

both the OBCPU/MMC and OBCPU groups could detect the down-regulated expression levels of the EGF gene and the SYPL2 gene, indicating that they might be closely associated with the function of the addition of PU (Fig. 7A and B). When comparing OBCPU/MMC with OBCPU, MMC might exert a related role by regulating heat shock family proteins and members of the MAPK-p38 family (Fig. 7C). Furthermore, we carried out KEGG and GO pathway enrichment analyses. We found that compared with the OBC group, both the OBCPU/MMC and OBCPU groups could be enriched in pathways such as mitochondrion, suggesting that the addition of PU might regulate mitochondrial function (Fig. 7D and E). Compared with OBCPU, OBCPU/MMC would impact protein folding, spatial conformation alterations, and the activity of TNF receptors, suggesting the potential role of MMC (Fig. 7F).

## 3. Discussion

The current range of treatments for urethral strictures is limited, especially regarding long and complex cases [1,31]. The repeated treatment process for urethral restenosis frequently has a significant financial and psychological impact on patients [32,33]. The treatment of urethral strictures based on tissue-engineered scaffolds has received widespread attention in recent years [12,34]. During the stricture process, the normal pseudostratified columnar epithelium is replaced by squamous metaplasia. The formation of small tears in the metaplastic tissue can result in the leakage of urine, which in turn leads to the replacement of the spongy body tissue with fibrous connective tissue. There is a notable increase in the ratio of type I to type III collagen, accompanied by aberrant alterations in the extracellular matrix [35,36]. Given the pivotal role of fibroblasts, particularly myofibroblasts, in urethral stricture formation, studies have demonstrated that MMC can effectively inhibit scar formation by fibroblasts without compromising epithelial cell growth [37]. Subsequent studies have shown that MMC can inhibit the transformation of fibroblasts into scar tissue and has a significant effect on the treatment of USD [23,38]. Accordingly, MMC was selected as the drug to be administered in this study. In our study, no

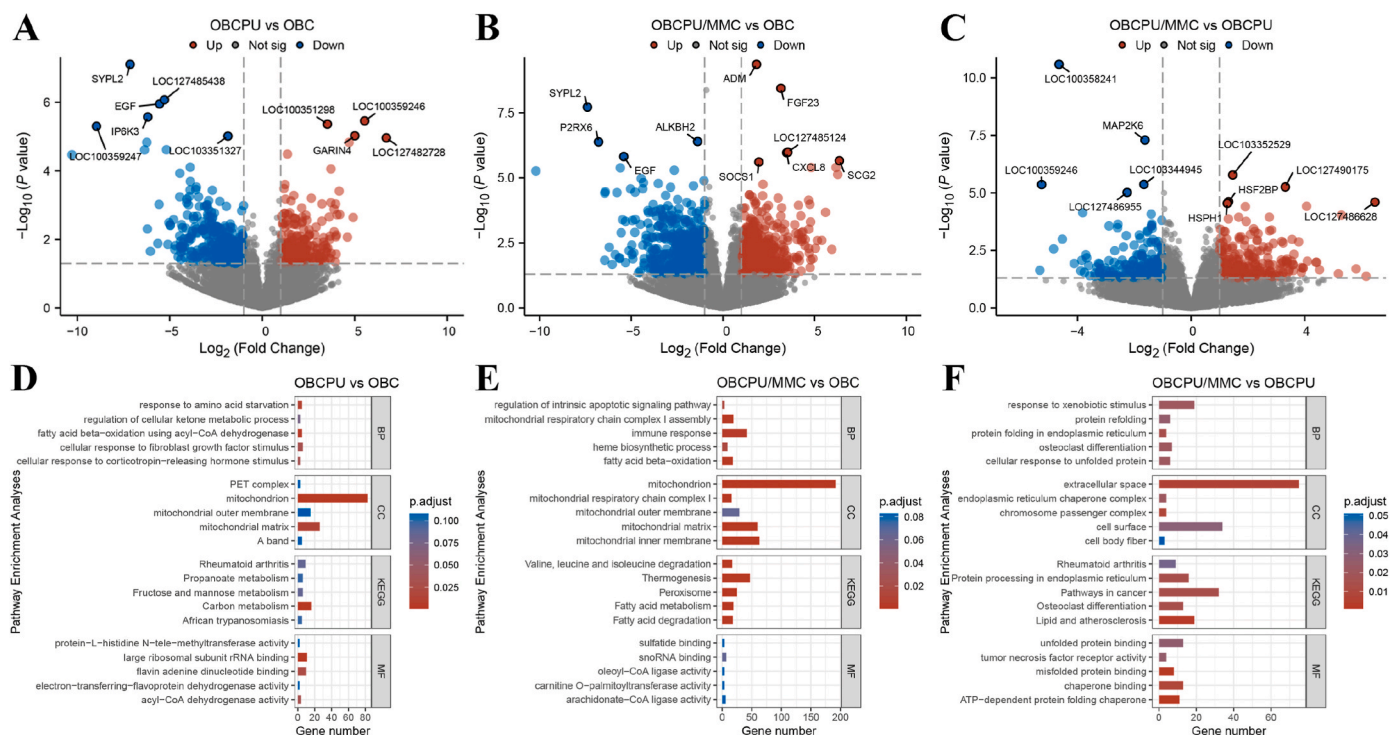


**Fig. 7.** Transcriptome analysis across diverse material groups: Analysis of differentially expressed genes in different groups, and the volcano plot is presented, (A) OBCPU vs OBC, (B) OBCPU/MMC vs OBC, (C) OBCPU/MMC vs OBCPU; Analysis of GO and KEGG pathway enrichment in different groups, (D) OBCPU vs OBC, (E) OBCPU/MMC vs OBC, (F) OBCPU/MMC vs OBCPU.



relevant toxicity of MMC on cells or adverse effects on tissue repair were detected, which could potentially be ascribed to the effect of sustained-release MMC. The experiments conducted on animals by other researchers also suggest that the continuous and sustained release of MMC could bring more benefits while reducing toxic and side effects [39].

The scaffold used for USD treatment was modified and synthesized using materials based on BC. Thanks to the presence of many amino acid esters on PU that can form hydrogen bonds, the modified scaffold exhibits excellent cytokine adsorption ability and improved cell adhesion properties. These attributes are crucial for promoting the regulation of the urethral microenvironment and facilitating the repair of tissue damage. Concurrently, the antibacterial properties of cationic PU have also been well demonstrated in previous studies [40,41]. The attachment of bacteria and the formation of extracellular polymers can have adverse effects on tissue recovery. Therefore, the ability of stents to inhibit bacteria in the urinary tract microenvironment is crucial. This material demonstrates good antibacterial effects against both *Escherichia coli* and *Staphylococcus aureus*. Although some articles have shown that MMC can affect the growth of some bacteria [42,43], our study did not find that MMC affects the common urethral colocalization flora, which may be related to the dose and release method of MMC.

Following the synthesis and verification of the scaffold, an *in vivo* validation was conducted using a New Zealand rabbit urethral defect model. The findings indicated that the OBCPU group demonstrated superior efficacy in repairing urethral strictures compared to the OBC group. Furthermore, the addition of MMC was found to significantly inhibit scar formation, which is in accordance with the findings of previous studies. The epithelial tissue in the OBCPU group was more complete, the vascularization was more abundant, and the urethra was observed to be similar in structure to normal urethral tissue. In this study, the OBCPU material demonstrated superior adsorption of various cytokines for early repair. However, further optimization of the follow-up related mechanism is required. At the mechanistic level, we initially discovered via microbes that the introduction of PU can indeed effectively exert antibacterial functions. However, the *in vitro* and *in vivo* experiments of MMC failed to confirm its antibacterial properties. In microbiomics analysis, the PU component can effectively inhibit *Escherichia coli*, which is relatively consistent with previous studies [44]. Further experiments are subsequently required to validate the potential value of microbiota in regulating urinary tract reconstruction.

Meanwhile, we found the changes of potential key genes and pathways between the materials through RNA-seq analysis. Firstly, a difference analysis was conducted among different groups. The results demonstrated that the introduction of PU could potentially lead to a relatively significant downregulation of EGF and SYPL2. SYPL2 might be closely associated with synaptic vesicles. Currently, there are relatively few related studies. Research indicates that it might be closely related to depression [45]. Moreover, EGF can prominently facilitate mitosis. The surgery was accomplished one month ago, at which time the samples were collected. PU might inhibit the continuous proliferation of certain scar-related cells, and this demands further investigation through single-cell sequencing in the subsequent process. The role of MMC might involve inhibiting cell proliferation, which is similar to its previous reports. We discovered in the results that the expression level of MAP2K6 was significantly downregulated, which might be related to the MAPK-p38 pathway [46]. Meanwhile, MMC can lead to a considerable upregulation of the expression levels of the members of the heat shock protein family, which might be associated with its potential cytotoxicity. At the level of pathway enrichment, PU might be closely associated with the mitochondrion. PU might exert antibacterial and other functions through causing alterations in mitochondrial function. MMC is enriched in certain pathways related to protein folding changes and changes in responses to the environment, which might be closely related to the potential toxicity of MMC, and these pathways might be the potential causes influencing the activation of fibroblasts to secrete ECM.

There are also several potential limitations of this study. Firstly, the materials in this experiment were designed in accordance with the pathological mechanism of urethral stricture. The relevant treatment was administered to the urethral defect model of New Zealand rabbits, but it could not fully mirror the actual situation of patients with urethral stricture in clinical practice. Subsequently, corresponding clinical trials need to be carried out for further exploration. Secondly, this study initially clarified the efficacy and safety of the material. The release of MMC reached the set dose within over one month. However, in the subsequent experiments, the observation period should be further prolonged to determine whether the MMC material has potential toxicity. Again, there is more to be investigated regarding how the design of related materials can release MMC more precisely in the subsequent process for inhibiting scar formation. Based on the above limitations, in the subsequent research, we will continue to advance the design and modification of this material and enhance the application method of the drug to make it more effectively applied to urethral stricture. In the subsequent studies, we intend to further investigate the design and modification of this material for bladder repair and ureter repair, and assess its efficacy.

#### 4. Conclusions

In conclusions, we designed and synthesized a BC-based scaffold with good biocompatibility for treating USD. This scaffold exhibits cytokines adsorption capacity and antibacterial properties, which can effectively provide a foundation for tissue regeneration. Meanwhile, the MMC loaded onto the stent demonstrated long-term drug release effects. Its efficacy has been verified in animal models. This scaffold offers novel concepts and approaches for the repair of urethral strictures.

#### 5. Materials and methods

##### 5.1. Treatment and oxidation of bacterial cellulose

All of the chemical reagents were of analytical reagent grade and used without further purification. Bacterial cellulose was provided by Hainan Yide Food Co., Ltd (China). Sodium hydroxide (NaOH), Oxalyl dihydrazone, Sodium periodate, ethylene glycol, isophorone diisocyanate, 2-isocyanatoethyl methacrylate and dibutyltin dilaurate were purchased from Shanghai Macklin Biochemical Co., Ltd (China).  $\beta$ -cyclodextrin, PEG 1000, 2-(Diethylamino) propane-1,3-diol and 1-Bromooctane and was acquired from Aladdin reagent Co., Ltd (China). Acetone were obtained from Beijing Chemical Works (China). PBS (pH 7.4, 10 mM) was purchased from Technologies Corporation (U.S.A.). Ultrapure water was from University of Science and Technology Beijing. fetal bovine serum (FBS), Dulbecco's modified Eagle's medium (DMEM) was purchased from Technologies Corporation (U.S.A.). Calcein-AM, propidium iodide (PI) were provided by Sigma-Aldrich (China). Cell Counting Kit-8 (CCK-8) was from Tongren Chemical Research Institute (Japan). *Escherichia coli*, *Staphylococcus aureus* was provided by ATCC (American Type Culture Collection). LB broth, LB and TSB medium agar were obtained from Beijing Aoboxing Biotechnology Co., Ltd (China). Crystal Violet Staining Solution, 2,3-Bis-(2-Methoxy-4 Nitro-5 Sulfo-phenyl)-2H Tetrazolium-5 Carboxanide (XTT), Fluorescent Brightener were purchased from Sigma-Aldrich (U.S.A.).

##### 5.2. Characterizations and instruments

The  $^1\text{H}$  NMR analysis were employed to investigate the preparation of products through NMR spectroscopy (Avance II 400 MHz, Bruker, Switzerland). FT-IR was carried out on Bruker TENSOR II (BRUKER, US, Germany). XRD was measured via a Bruker D8 ADVANCE X (Bruker, Germany). The  $\zeta$ -potential were performed via the Malvern Zsizer Nano ZS90 system (Malvern, UK). The Differential Scanning Calorimetry (DSC) was carried out at DSC 2500 (TA Instruments, USA). The



morphologies of nanoparticles were observed through scanning electron microscope (SEM, G300, Zeiss, Jena, Germany). Static contact angle was carried out on OCA15EC (Dataphysics, Germany). Mechanical properties were tested by TA-XT plus (SMS, UK). The UV–vis absorption was obtained via a Lambda850 (Perkinlmer, U.S.A.). Colorimetric experiment was carried out on Multiskan MK3 (ThermoFisher, U.S.A.). The fluorescence images of cells were obtained from a inverted fluorescence microscope (Leica, Germany).

### 5.3. Synthesis and processing of OBCPU

BC with a thickness of 3 mm was immersed in a 0.1 mol/L NaOH solution and boiled at 100 °C for 1 h. It was then repeatedly rinsed and cleaned with deionized water until the pH stabilized at approximately 7.2. Following this, the BC was placed in a sodium periodate solution and stirred gently at room temperature in the dark. The product was subsequently immersed in a 0.1 mol/L glycol solution for 0.5–1 h to remove any residual sodium periodate. This process resulted in the formation of Oxidized Bacterial Cellulose (OBC). Cut OBC into  $2 \times 2$  cm thin sheets. 10 pieces of OBC were placed in 20 mL of a solution containing PU at a concentration of 0.1 g/mL and iCD at 0.025 g/mL and stirred at 60 °C for 8 h. Afterward, it was washed in PBS to obtain PU crosslinked OBC, referred to as OBCPU. The synthesis of PU and iCD is depicted in [Scheme S1-2](#).

### 5.4. Water vapor transmission rate of OBCPU

The film was cut into circular specimens with a radius of 1.0 cm, and surface-free water was removed by the vertical suspension method. A 15 mL centrifuge tube was prepared with a circular hole of 1 cm diameter on the cap. Sufficient water was added to the tube to create a 5 mm gap between the liquid level and the air after the sample was placed. The sample was accurately covered on the concave edge of the container, clamped tightly without deformation, and the total mass of the system was measured. The centrifuge tube was placed upright on the sample, and the conditions were maintained at 37 °C with a relative humidity below 20 %. The weight change  $\Delta W$  was recorded every 6 h for 48 h. The water vapor permeability was calculated by the ratio of weight change to pore area, and the average was taken from three samples per group.

### 5.5. Mechanical Property test of OBCPU

The film was cut into  $1 \times 1$  cm<sup>2</sup> sheets, frozen in a –20 °C refrigerator and placed in a freeze-drying machine for 1 day, after which its morphology was observed through SEM. The film was then cut into dumbbell-shaped standard samples using a punch, and the stress-strain curve was measured at a testing speed of 1.5 mm/s. Test results were considered valid even if the narrow part of the sample broke during stretching. Tear strength specimens were prepared as pants-shaped according to the standard 'ISO 13937-2:2000 Textiles Tear properties of fabrics'. From each group, three identical specimens with a thickness of 2 mm were selected. These specimens were then subjected to a tensile test at a speed of 1.5 mm/s until complete tearing occurred. A tear at the normal pre-crack position was considered valid for testing processes. The experimental environment was maintained at a temperature of 25 °C and a humidity of 70 %.

Place the film on the opening of the rupture strength testing machine, use a 5.0 mm spherical probe to puncture the sample at a speed of 500 mm/min, and detect the stress during puncture.

### 5.6. Calculation details

The molecular sketches of all compounds were drawn using Material Studio 2020.

The establishment of boxes for BC, OBC and OBCPU and double layer with VEGF. After balancing the model, the CVFF force field was used to

export the model, which is further calculated using LAMMPS. Perform a 100ps NPT calculation at 310K until equilibrium. Statistically analyze the cohesive energy density and non-bond energy changes and select snapshots at different stages through VMD.

DFT calculations were performed using Gaussian 16, and molecules were optimized using B3LYP for geometric structure. The basis-set defines different elements separately, with most elements selected as the 6–31g (d', p') basis-set for calculation. The calculation of the total electron density is a further essential step. The binding energy is then calculated by means of optimizing different structures.

### 5.7. Load and release of MMC

A quantity of 200 µg of MMC is to be dissolved in PBS, following which the solution is to be mixed thoroughly. Subsequently,  $1 \times 1$  cm<sup>2</sup> pieces of BC, OBC, and OBCPU were placed into the solution and stirred at 37 °C for 24 h prior to being rinsed with PBS. The MMC loading rate is then calculated by measuring the change in absorption at 365 nm using UV spectroscopy.

Samples loaded with MMC were maintained in PBS at a stable temperature and humidity of 37 °C. The MMC loading rate was then monitored over a 1-month period using UV spectroscopy.

### 5.8. Cytotoxicity and MMC release performance test

Perform experiments utilizing endothelial cells. Seed the cells at a density of  $1 \times 10^5$  cells per well in a 96-well plate and culture them using extraction solutions from BC, OBC, and OBCPU. Cell survival rates from each group were assessed at 1, 4, and 7 days using the CCK-8 assay. Additionally, the cell viability and distribution were visualized through live and dead staining. The cells were then seeded onto the surfaces of BC, OBC, and OBCPU to evaluate cellular activity on the material surfaces. The CCK-8 assay should be used to monitor cell activity, and the cytoskeleton should be stained to observe cell morphology. Finally, glucose metabolism activity should be measured to assess cellular metabolic function.

### 5.9. Antibacterial property test

The antibacterial activity was evaluated through the cultivation of Escherichia coli (E. coli) and Staphylococcus aureus (S. aureus) on agar plates, followed by the observation of the inhibition zones surrounding three distinct film types within the culture medium. The quantification of antibacterial efficacy was achieved by determining the colony forming units (CFU). Bacterial solutions were diluted to achieve a concentration of  $10^6$  CFU/mL. Aliquots of 100 µL were then diluted 10,000-fold and spread evenly onto agar plates. After a further 24-h incubation at 37 °C, the number of colonies was counted by photographing the agar plates. SEM was utilized to examine the morphology of bacteria on the surfaces of the different materials.

### 5.10. Anti-biofilm test

To study biofilm formation, we added bacterial solutions to a 96-well plate and observed it at 12 and 24 h. Following this, the biofilms were stained with crystal violet after washing with water and dried. We then added crystal violet dye, waited 15 min, and checked the biofilm under a microscope. After rinsing with alcohol, we measured the dye's absorbance at 595 nm. For testing biofilm activity, we made an XTT dye solution by mixing XTT and benzoquinone. We added this dye and PBS to the wells and let them sit in the dark for 2 h at 37 °C. We then transferred some liquid to a new plate and measured its absorbance at 490 nm to assess the activity.



### 5.11. Construction of a urethral defects model in New Zealand rabbits

The study received ethical approval from the Animal Ethics Committee of Peking University First Hospital (J2023057). The male New Zealand rabbits weighing between 2.5 and 3.5 kg were procured and placed in an appropriate feeding environment. The night preceding surgery, the experimental animals were deprived of both food and water. Some surgical process images are shown in Fig. S15. The vein along the ear margin was anaesthetized with sodium pentobarbital, and an 8F urinary catheter was left in situ. The urethral defect was incised 1.5 cm downward along the head of the penis at 0.5 cm, and the urethra was exposed by incising the subcutaneous tissue in a meticulous, layer-by-layer manner. Then the scaffold was trimmed to match the defect size and subsequently positioned with precision onto the defect site. The patch edges were secured to the native urethral tissue using 5-0 absorbable sutures in an interrupted pattern. The New Zealand rabbits were randomly divided into four groups, with five rabbits in each group: a. Control group, where a urethral defect was created and directly sutured without any additional intervention; b. OBC group, where the urethral defect was repaired using an oxidized bacterial cellulose (OBC) scaffold; c. OBCPU group, where the urethral defect was repaired using an OBCPU scaffold; d. OBCPU/MMC group, where the urethral defect was repaired using an OBCPU/MMC scaffold. After surgery, the New Zealand rabbits were fitted with an Elizabethan collar and a urinary catheter for a period of one week, and long-acting antibiotics were injected to prevent infection.

### 5.12. Imaging and histological evaluation

The model animals were analyzed by imaging evaluation at the end time point after surgery. Firstly, the animals were anaesthetized, and an ultrasound evaluation of the urethra was conducted using an ultrasound device. Subsequently, an ureteroscope was employed to monitor the urinary tract. Finally, the urethrography was performed using iodopromide to assess the condition of urethral stricture in the New Zealand rabbits. We then euthanized the model animals and obtained urethral tissue for preparation of Paraffin sections. After that, we condemned the Masson, HE, Sirius red and TNF- $\alpha$  detection to verify the urethral repair, fiber arrangement and inflammatory infiltration.

### 5.13. Analysis of urethral tissue flora

After the animals were terminated, urethral tissue was obtained for 16S rRNA sequencing analysis. By using feature data, sequence comparisons with the 16S databases SILVA and NT-16S could be conducted to identify and annotate species at multiple taxonomic levels, ranging from Kingdom, Class, Order, Family, Genus to Species of the 16S sequences detected in the sample. Subsequently, we identified the  $\alpha$  and  $\beta$  diversity of the flora and carried out an analysis of significantly different flora. Then we clarified the flora situation between different groups and confirmed the efficacy of the antibacterial scaffold. At the same time, we performed Bugbase and LSfSE analyses to identify potential differences in the flora, and KEGG analysis to look for potential functions of the diverse flora.

### 5.14. Bioinformatics analysis of different groups

We procured urethral tissues of New Zealand rabbits from the OBC, OBCPU, and OBCPU/MMC groups and extracted cDNA using the Trizol method [47]. Subsequently, the cDNA was subjected to RNA sequencing via the illumina X plus platform to identify differential genes and potential biological pathway enrichments among the different groups. Then, the differential gene expressions among different groups were analyzed through the DESeq2 package and the pathway enrichment through the clusterprofiler package in the R environment [48,49]. Genes or pathways with a p-value <0.05 were identified as significant and

utilized for subsequent graphical analysis and presentation.

### CRediT authorship contribution statement

**Zhenpeng Zhu:** Writing – original draft, Formal analysis, Conceptualization. **Jianming Zhao:** Writing – original draft, Methodology, Formal analysis. **Xing Ji:** Writing – review & editing, Investigation. **Weimin Hu:** Methodology, Investigation, Formal analysis. **Wenyuan Leng:** Investigation, Formal analysis. **Chunru Xu:** Software. **Xiaoyu Li:** Software. **Kunlin Yang:** Resources, Data curation. **Xuesong Li:** Supervision, Investigation. **Yudong Zheng:** Writing – review & editing, Supervision, Resources. **Jian Lin:** Writing – review & editing, Resources, Conceptualization.

### Data availability

All the data of this study can be acquired from the corresponding author upon reasonable request.

### Ethics approval and consent to participate

All the animal research processes were approved and supervised by the Animal Ethics Committee of Peking University First Hospital (Permission number: J2023057). All authors were compliance with all relevant ethical regulations.

### Declaration of competing interest

All authors declare that they have no conflict of interest.

### Acknowledgments

This work was supported by grants from the National Natural Science Foundation of China (No. 82070704, No. 82270708, and No. 52273119); National High Level Hospital Clinical Research Funding (Youth Clinical Research Project of Peking University First Hospital No. 2023YC16).

### Appendix A. Supplementary data

Supplementary data to this article can be found online at <https://doi.org/10.1016/j.bioactmat.2025.04.031>.

### References

- [1] N. Lumen, et al., European association of urology guidelines on urethral stricture disease (Part 1): management of male urethral stricture disease, *Eur. Urol.* 80 (2) (2021) 190–200.
- [2] H. Wessells, et al., Urethral stricture disease guideline amendment (2023), *J. Urol.* 210 (1) (2023) 64–71.
- [3] M.D. Grimes, et al., Histopathology of anterior urethral strictures: toward a better understanding of stricture pathophysiology, *J. Urol.* 202 (4) (2019) 748–756.
- [4] M. Li, et al., Cell sheet formation enhances the therapeutic effects of adipose-derived stromal vascular fraction on urethral stricture, *Mater. Today Bio* 25 (2024) 101012.
- [5] A. Simsek, et al., Overcoming scarring in the urethra: challenges for tissue engineering, *Asian J Urol* 5 (2) (2018) 69–77.
- [6] S. Tritschler, et al., Urethral stricture: etiology, investigation and treatments, *Dtsch Arztebl Int* 110 (13) (2013) 220–226.
- [7] S. Kim, et al., Antibiotic stewardship and postoperative infections in urethroplasties, *Urology* 152 (2021) 142–147.
- [8] K. Zhang, et al., microRNA expression profiles of scar and normal tissue from patients with posterior urethral stricture caused by pelvic fracture urethral distraction defects, *Int. J. Mol. Med.* 41 (5) (2018) 2733–2743.
- [9] S. Fan, et al., Biomaterial-based scaffolds as antibacterial suture materials, *ACS Biomater. Sci. Eng.* 6 (5) (2020) 3154–3161.
- [10] I.J. Abbott, et al., Antibiotic management of urinary tract infections in the post-antibiotic era: a narrative review highlighting diagnostic and antimicrobial stewardship, *Clin. Microbiol. Infection* 29 (10) (2023) 1254–1266.
- [11] H. Luo, et al., Pharmacotherapy of urethral stricture, *Asian J. Androl.* 26 (1) (2024) 1–9.



- [12] N. Chepelova, et al., The search for an optimal tissue-engineered urethra model for clinical application based on preclinical trials in male animals: a systematic review and meta-analysis, *Bioeng Transl Med* 9 (6) (2024) e10700.
- [13] E. Palminteri, et al., Long-term results of small intestinal submucosa graft in bulbar urethral reconstruction, *Urology* 79 (3) (2012) 695–701.
- [14] M. Casarin, A. Morlacco, F. Dal Moro, Tissue engineering and regenerative medicine in pediatric urology: urethral and urinary bladder reconstruction, *Int. J. Mol. Sci.* 23 (12) (2022).
- [15] Y. Jin, et al., Multilayered hydrogel scaffold construct with native tissue matched elastic modulus: a regenerative microenvironment for urethral scar-free healing, *Biomaterials* 312 (2025) 122711.
- [16] F. Wahid, et al., Bacterial cellulose and its potential for biomedical applications, *Biotechnol. Adv.* 53 (2021) 107856.
- [17] A. Prilepskii, V. Nikolaev, A. Klaving, Conductive bacterial cellulose: from drug delivery to flexible electronics, *Carbohydr. Polym.* 313 (2023) 120850.
- [18] Z. Zhu, et al., Clinical application of a double-modified sulfated bacterial cellulose scaffold material loaded with FGFR2-modified adipose-derived stem cells in urethral reconstruction, *Stem Cell Res. Ther.* 13 (1) (2022) 463.
- [19] X. Zhao, et al., Barnacle-inspired and polyphenol-assisted modification of bacterial cellulose-based wound dressings for promoting infectious wound healing, *Int. J. Biol. Macromol.* 279 (Pt 2) (2024) 135291.
- [20] A.K. Saleh, et al., Functionalization of bacterial cellulose: exploring diverse applications and biomedical innovations: a review, *Int. J. Biol. Macromol.* 264 (Pt 1) (2024) 130454.
- [21] H. Sawires, et al., Early topical mitomycin-C prevents stricture formation in children with caustic ingestion, *J. Paediatr. Child Health* 60 (9) (2024) 402–408.
- [22] P. Wu, et al., Characteristics of mitomycin C-loaded peptide hydrogel in vitro and anticarring effects in rat ocular injury model, *J. Ocul. Pharmacol. Therapeut.* 39 (2) (2023) 139–147.
- [23] R. Klein, et al., Minimally invasive management of posterior urethral stricture/stenosis with DVIU and mitomycin C injection, *Urology* 183 (2024) e317–e319.
- [24] F.H. Pranata, et al., The efficacy and safety of mitomycin C intra urethral injection to prevent recurrent urethral stricture: a systematic review and meta-analysis, *Ann. Med. Surg.* 77 (2022) 103576.
- [25] F.V.A. Dutra, et al., Coumarin/ $\beta$ -Cyclodextrin inclusion complexes promote acceleration and improvement of wound healing, *ACS Appl. Mater. Interfaces* 16 (24) (2024) 30900–30914.
- [26] Y. Wang, et al., Calixarene-modified albumin for stoichiometric delivery of multiple drugs in combination-chemotherapy, *Theranostics* 12 (8) (2022) 3747–3757.
- [27] N.G. Hädärugä, et al., A review on thermal analyses of cyclodextrins and cyclodextrin complexes, *Environ. Chem. Lett.* 17 (1) (2019) 349–373.
- [28] F. Seidi, Y. Jin, H. Xiao, Polycyclodextrins: synthesis, functionalization, and applications, *Carbohydr. Polym.* 242 (2020) 116277.
- [29] Y. Huang, et al.,  $\gamma$ -Cyclodextrin metal-organic frameworks as the promising carrier for pulmonary delivery of cyclosporine A, *Biomed. Pharmacother.* 171 (2024) 116174.
- [30] J. Hu, et al., Reduction-triggered polycyclodextrin supramolecular nanocage induces immunogenic cell death for improved chemotherapy, *Carbohydr. Polym.* 301 (2023) 120365.
- [31] Y. Jin, et al., Scaffold-based tissue engineering strategies for urethral repair and reconstruction, *Biofabrication* 17 (1) (2024).
- [32] Y. Yan, et al., Impact of a clinical care pathway developed through the action research method on the psychological well-being and quality of life in male patients with urethral stricture, *Medicine (Baltim.)* 103 (9) (2024) e37321.
- [33] M.J. Jackson, S.L. Ivaz, Quality and length of life, money and urethral stricture disease, *Curr. Opin. Urol.* 25 (4) (2015) 346–351.
- [34] M. Habibzadeh, et al., Engineered tissues: a bright perspective in urethral obstruction regeneration, *Tissue Eng., Part B* (2024).
- [35] M. Singh, J.P. Blandy, The pathology of urethral stricture, *J. Urol.* 115 (6) (1976) 673–676.
- [36] E.C. Linssen, et al., Extracellular matrix analysis of fibrosis: a step towards tissue engineering for urethral stricture disease, *PLoS One* 18 (11) (2023) e0294955.
- [37] I.Y. Chang, et al., Morphological effects of mitomycin C on urothelial responses to experimentally-induced urethral stricture in rats, *Int. J. Urol.* 22 (7) (2015) 702–709.
- [38] O. Kurt, et al., Effect of mitomycin - C and triamcinolone on preventing urethral strictures, *Int. Braz. J. Urol.* 43 (5) (2017) 939–945.
- [39] R.J.S. van Mechelen, et al., A degradable sustained-release drug delivery system for bleb-forming glaucoma surgery, *Macromol. Biosci.* 23 (10) (2023) e2300075.
- [40] Z. Zeng, et al., Bioadhesive first-aid patch with rapid hemostasis and high toughness designed for sutureless sealing of acute bleeding wounds, *Adv. Healthc. Mater.* (2024) e2403412.
- [41] J. Zhang, et al., Quercetin@ $\beta$ -Cyclodextrin conjugated keratin/polyurethane biocomposite mats for infected diabetic wound healing, *Langmuir* 40 (45) (2024) 23673–23682.
- [42] O. Pacios, et al., Mitomycin C as an anti-persister strategy against *Klebsiella pneumoniae*: toxicity and synergy studies, *Antibiotics (Basel)* 13 (9) (2024).
- [43] E. Svedholm, et al., Repurposing mitomycin C in combination with pentamidine or gentamicin to treat infections with multi-drug-resistant (MDR) *Pseudomonas aeruginosa*, *Antibiotics (Basel)* 13 (2) (2024).
- [44] A.H. Rather, et al., Polyurethane and cellulose acetate micro-nanofibers containing rosemary essential oil, and decorated with silver nanoparticles for wound healing application, *Int. J. Biol. Macromol.* 226 (2023) 690–705.
- [45] K. Torii, et al., Tissue-specific gene expression of genome-wide significant loci associated with major depressive disorder subtypes, *Prog. Neuropsychopharmacol. Biol. Psychiatry* 133 (2024) 111019.
- [46] J. Lv, et al., Inhibitory impact of prenatal exposure to nano-polystyrene particles on the MAP2K6/p38 MAPK Axis inducing embryonic developmental abnormalities in mice, *Toxics* 12 (5) (2024).
- [47] D.C. Rio, et al., Purification of RNA using TRIzol (TRI reagent), *Cold Spring Harb. Protoc.* 2010 (6) (2010) pdb.prot5439.
- [48] M.I. Love, W. Huber, S. Anders, Moderated estimation of fold change and dispersion for RNA-seq data with DESeq2, *Genome Biol.* 15 (12) (2014) 550.
- [49] G. Yu, et al., clusterProfiler: an R package for comparing biological themes among gene clusters, *OMICS* 16 (5) (2012) 284–287.